Electronic structure models of phosphorus δ-doped silicon

Damien J. Carter,[1] Oliver Warschkow,[1] Nigel A. Marks,[2] and David R. McKenzie[1]
[1]*Centre for Quantum Computer Technology, School of Physics, The University of Sydney, Sydney, NSW 2006, Australia*
[2]*Nanochemistry Research Institute, Curtin University of Technology, P.O. Box U1987, Perth WA 6845, Australia*
(Received 2 November 2008; published 29 January 2009)

We report a density-functional theory treatment of phosphorus δ-doped silicon. Using large asymmetric unit cells with up to 800 atoms, we obtain first-principles doping potentials, band energies, and donor-electron distributions. The explicit and nonempirical description of both valence and donor electrons improves upon previous models of this system. The effects of overlapping δ-doping potentials in smaller systems are adequately captured using a uniform band alignment shift.

DOI: 10.1103/PhysRevB.79.033204 PACS number(s): 61.72.uf, 71.20.Mq, 71.20.Nr, 71.55.Cn

Delta doping describes the process in which the placement of dopant atoms is limited to a narrow plane in the host material.[1,2] This creates an approximately V-shaped doping potential in the plane-perpendicular direction, in which electron or hole carriers are trapped to form two-dimensional gases with a number of technologically useful properties.[3,4] Phosphorus δ-doped silicon is particularly interesting for its relevance to nanoelectronic device fabrication including the possibility of quantum computers.[5–7] Various prototype Si:P devices are currently being developed[5,8–15] in which patterned δ-doped layers form conducting leads and gate electrodes. These developments warrant and motivate detailed theoretical studies into the baseline electronic properties of phosphorus δ-doped silicon. A particular difficulty of this system is associated with the significant delocalization lengths of donor electrons in the host. Building on earlier theory work based on the effective-mass approximation,[16–19] the current benchmark understanding of δ-doped silicon is set by the work of Chang and co-workers.[20,21] Cartoixà and Chang[21] described conduction electrons using an empirical tight-binding model while Qian, Chang, and Tucker[20] (QCT) developed a conduction-band model based on density-functional theory (DFT). In this Brief Report we will show that phosphorus δ-doped silicon is now within the reach of full density-functional theory, thus realizing a complete and nonempirical treatment of both valence and donor electrons.

We describe δ-doped silicon using large periodic superlattices in the [001] direction [Fig. 1(a)]. In order to assess (and minimize) the interaction between successive δ-layers, we consider highly asymmetric supercells with a long periodic repeat between 40 and 200 atomic layers (55 and 275 Å, respectively). For the in-plane directions, we use three different unit cells with 4, 8, and 16 atoms per atomic plane. A $c(2\times2)$ cell [Fig. 1(b)] describes phosphorus donor densities of 1/4, 1/2, and 1 monolayer (ML). A $p(2\times2)$ cell [Fig. 1(b)] is used to describe a 1/8 ML donor density. A large $c(4\times4)$ cell [Fig. 1(c)] is used to explore the effects of disorder in the in-plane placement of donors. Geometry optimization of the coordinates was not performed.[22] Reciprocal space integrations for these cells are performed using $4\times4\times1$, $3\times3\times1$, and $2\times2\times1$ **k**-point grids, respectively. These are sufficiently converged such that the energy difference is less than 0.6 meV/atom.

Our calculations are performed using the SIESTA (Ref. 23) software in which the electronic eigenfunctions are expanded in localized atomic basis set. In order to access very large systems, we used single numerical plus polarization basis sets together with a norm-conserving pseudopotential for 1*s* electrons.[24] Exchange-correlation energies are calculated using the Perdew-Burke-Ernzerhof (PBE) functional[25] and are evaluated on a real-space grid (cutoff 300 Ry). With these computational settings, the calculated bulk silicon lattice parameter of $a=5.500$ Å compares favorably with the experimental value[26] of $a=5.431$ Å. The calculated band gap of 0.79 eV is indirect with the valence-band maximum (VBM) at the Γ point and the conduction-band minima (CBM) at $k_\Delta^{(1\times1)}=\pm0.843(2\pi/a)$. For the δ-doped cells, we report all band energies and Fermi levels (E_F) relative to the bulk CBM. This necessitates a band alignment between δ-doped and bulk (undoped) silicon which is achieved by matching the averaged electrostatic potentials in the atomic plane most distant from the δ layer. This type of alignment assumes that the δ-doping potential has vanished at the matching plane. To the extent that this is not the case, an error is introduced that we refer to as an *alignment shift* (AS). We will estimate the size of this error and discuss its effects below.

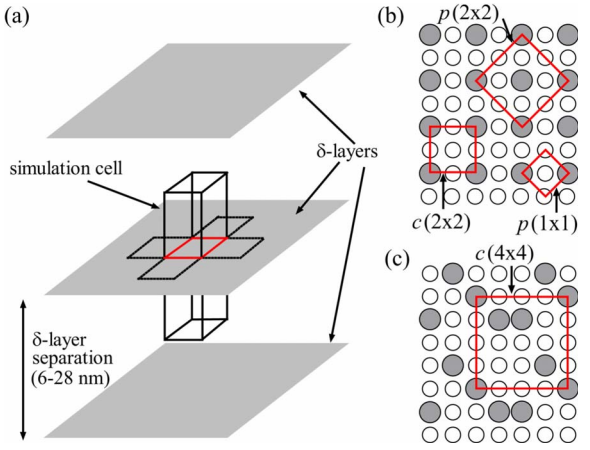

FIG. 1. (Color online) (a) Schematic of the three-dimensional (3D) periodic superlattices used to represent δ doping in this work. (b) Plane view of a δ-doped atomic layer containing 1/4 ML phosphorus (shaded circles) in an ordered $c(2\times2)$ arrangement. $p(1\times1)$ and $p(2\times2)$ unit cells are indicated for reference. (c) Plane view of a 1/4 ML δ-doped layer with phosphorus atoms in a quasidisordered arrangement with $c(4\times4)$ periodicity.

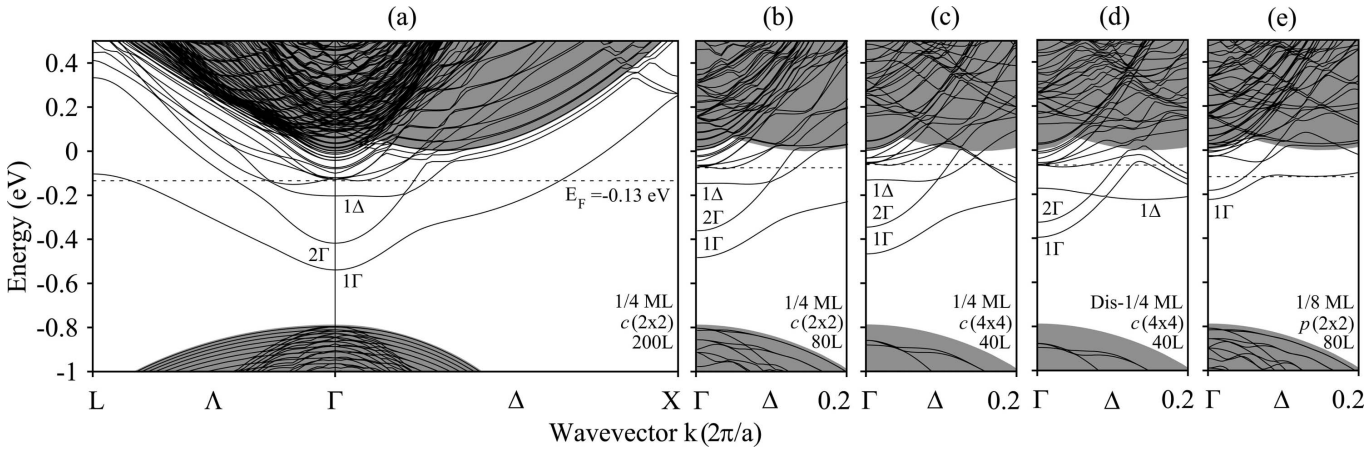

FIG. 2. Band structures of the 1/4 ML phosphorus δ-doped layer in the (a) 200L and (b) 80L supercells. Band structures of the 1/4 ML (c) ordered and (d) disordered phosphorus δ-doped layers in the $c(4\times4)$ supercells that contain 40 atomic planes. (e) Band structure of the 1/8 ML phosphorus δ-doped layer in the 80L supercell. The plane projected bulk band structure of Si is represented by the gray continuum. The Fermi level is indicated by a horizontal dashed line.

Figure 2(a) shows the calculated band structure for a 1/4 ML phosphorus δ-doped layer in our largest supercell with 200 atomic layers (denoted 200L in the following). For orientation, the projected bulk band structure is shown as a gray-shaded background. In the $c(2\times2)$ unit cell used, the six bulk conduction-band minima are folded such that the four in-plane minima appear at $k_\Delta^{c(2\times2)}=1-k_\Delta^{(1\times1)}=0.157(2\pi/a)$ and the two out-of-plane minima appear at the Γ point. The discrete bands shown are those of a 1/4 ML δ-doped layer in the 200L model. We see several conduction bands pulled into the bulk band gap by the doping potential. The lowest two, labeled 1Γ and 2Γ, have their minima at the Γ point; these correspond to the out-of-plane minima of bulk silicon. Further up, we find the fourfold-degenerate in-plane minima labeled 1Δ. All of these discrete bands are partially occupied, crossing the Fermi level E_F at −0.13 eV. Broadly, our band structure is in good agreement with the conduction-band-only results of the QCT model.[20] Our calculated band minima for 1Γ and 2Γ at −0.54 and −0.42 eV, respectively, compare favorably to the QCT result (both near −0.4 eV). Also in good agreement is the Fermi energy which QCT report as −0.099 eV.

Figures 2(b) and 2(c) examine the effect of a reduced separation between successive δ layers using smaller superlattices of 80 and 40 layers (80L and 40L, respectively). In comparison with the 200L model [Fig. 2(a)], we see that the band structure of the δ-doped layer is well preserved in the smaller models except for a small upshift in energy relative to the CBM. This is quantified in Table I where we report the calculated Fermi level, as well as the band minima of 1Γ, 2Γ, and 1Δ for five superlattice sizes. Comparing the 160L and 200L models, differences in the band energies are below 0.02 eV. The results for the 80L model are within 0.06 eV of the 200L model, giving a sense of the degree of convergence achieved. We further observe that *differences* between band energies (e.g., 2Γ−1Γ) are much better converged, supporting the idea of a uniform shift.

These energy shifts can be understood by considering the self-consistent doping potential, calculated here as the electrostatic potential difference between δ-doped and undoped supercells. Figure 3 shows an overlay of plane-averaged doping potentials obtained for five superlattice models. The potential for the largest model (200L) is aligned to zero (the bulk CBM) at the point furthest from the δ layer. The calculated Fermi level as well as the 1Γ, 2Γ, and 1Δ band minima of this model are included for reference. The doping potentials of the 40L, 80L, 120L, and 160L models are shifted such that they match the 200L potential in the vicinity of the δ layer. This shows that, near the δ layer, the doping potentials match almost exactly, irrespective of the superlattice model used. However, further away the doping potentials diverge with the smaller models flattening out earlier and toward lower potentials. This is caused by the periodic doping potential implicit in our supercell representation; the attractive wells of adjacent δ layers overlap, leading to an artificial lowering of the potential. The dotted curves on the right-hand side of Fig. 3 illustrate this effect for the 40L and 80L models. Since our alignment with the bulk CBM assumes the doping potential to have vanished to zero at the atomic plane furthest from the δ layer, the overlapping doping potentials in smaller systems will result in a net upward shift. We can estimate the size of this effect by referencing

TABLE I. E_F, 1Γ, 2Γ, 1Δ, and the VBM, for 1/4 ML δ doping in the 40L, 80L, 120L, 160L, and 200L supercells. Also given is the alignment shift (AS_{200}) that matches the doping potential of the model with that of the larger 200L model in the vicinity of the δ layer.

Supercell	40L	80L	120L	160L	200L
E_F (eV)	−0.06	−0.08	−0.11	−0.12	−0.13
1Γ (eV)	−0.47	−0.48	−0.51	−0.53	−0.54
2Γ (eV)	−0.35	−0.36	−0.39	−0.41	−0.42
1Δ (eV)	−0.14	−0.15	−0.18	−0.19	−0.21
VBM (eV)	−0.86	−0.80	−0.80	−0.80	−0.80
AS_{200} (eV)	−0.08	−0.06	−0.03	−0.01	0

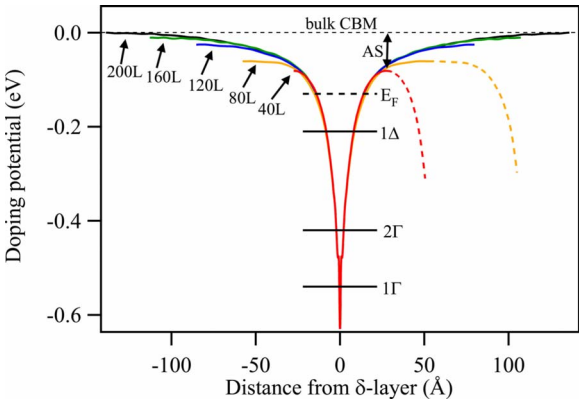

FIG. 3. (Color online) Self-consistent doping potential of a 1/4 ML δ-doped layer for various superlattice models. The plane-averaged potential furthest from the δ layer defines the zero reference for the 200L model. The potentials of the other supercell models are aligned to match the 200L potential in the vicinity of the δ layer. The Fermi level (E_F) of the 200L model, as well as the band minima of 1Γ, 2Γ, and 1Δ are also indicated. The AS (see text) is indicated for the 40L model.

the potential at the boundary for a given model to that of our largest model (200L). This quantity, hereafter referred to as the AS, is listed in Table I and can be seen closely matching the observed shift in the discrete doping bands. This observation of a uniform shift in these bands is physically intuitive given that even for the smallest model (40L) the doping potential is well converged up to and beyond the Fermi level (see Fig. 3).

Figure 4 provides a real-space visualization of a δ-doped layer, correlating the atomic geometry in panel (a) with the local density of states (LDOS) and the donor-electron distribution in panels (b) and (c). High and low values of the LDOS are shown in light (red) and dark (blue) colorations, highlighting the distortion of the band gap [i.e., the dark (blue) region] in the vicinity of the δ layer. Panel (b) is overlaid with the self-consistent doping potential (solid white curves) showing how the potential resembles the distortion seen in the conduction-band and valence-band edges. The distortion leads to spatial confinement of the discrete doping levels as demonstrated by several high-LDOS (red) stripes in the band gap below the Fermi level. Panel (c) shows the plane-averaged donor-electron distribution associated with these levels, obtained by integrating the LDOS between VBM and E_F.

Figure 5 shows how the donor-electron distribution changes when the phosphorus dopant density n_{2D} varies between 1/8 and 1 ML. As quantified in Table II, the maximum donor density ρ_{max} increases sharply with the dopant density. Furthermore, the increase is above proportional due to an increasingly confining δ potential. Correspondingly, the width of the distribution decreases with dopant density as seen by the reduction in the width at half maximum ($\rho_{max}/2$) from 10 Å for the 1/8 ML case to 2.7 Å for 1 ML. Note that the base width of the distributions (heuristically quantified by $\rho_{max}/10$) is considerably larger: between 34 and 12 Å. The deepening of the doping potential is also evident in the band energies in Table II, which steadily decrease with dop-

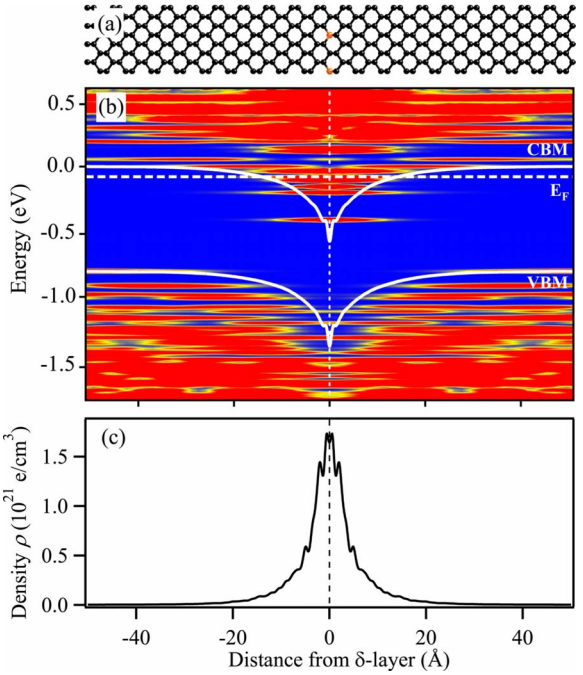

FIG. 4. (Color online) Electronic structure results for a 1/4 ML phosphorus δ-doped layer in silicon (80L model): (a) structure model, (b) local density of states as a function of distance from the δ layer [dark (blue) and light (red) colored regions represent low and high density of states, respectively], and (c) self-consistent donor-electron distribution. The self-consistent doping potential is superimposed on panel (b) as a white curve. The vertical dotted line indicates the phosphorus-doped atomic plane.

ant density. The Fermi level however remains largely unchanged due to the counteracting effect of an increasing number of donor electrons. These changes are evident also in the 1/8 ML band-structure diagram in Fig. 2(e), which are upshifted due to a less attractive δ layer. For the 1/4, 1/2, and 1 ML systems, it was feasible to compute the AS_{200} potential alignment shift and it was found to be insensitive to the doping density.

Finally, we consider with Figs. 2(c) and 2(d) the effect of dopant disorder on the electronic structure. Figure 1 illus-

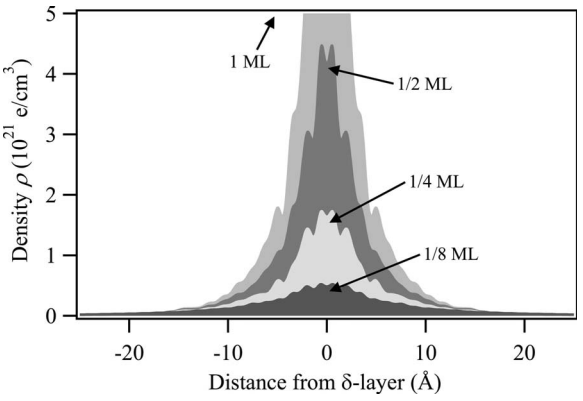

FIG. 5. Plane-averaged distribution of donor electrons for a δ-doped layer containing between 1/8 and 1 ML phosphorus in a 80L supercell model.

TABLE II. Calculated Fermi-level E_F, band minima (1Γ, 2Γ, 1Δ), VBM, and maximum donor-electron density ρ_{max} as a function of the phosphorus dopant density n_{2D} in the δ layer. These results were obtained for the $80L$ supercell model.

n_{2D} (ML)	1/8 ML	1/4 ML	1/2 ML	1 ML
ρ_{max} (10^{21} e/cm^3)	0.5	1.7	4.5	12.6
Width (Å) at $\rho_{max}/2$	10	6.7	5.3	2.7
Width (Å) at $\rho_{max}/10$	34	20	16	12
E_F (eV)	−0.12	−0.08	−0.08	−0.09
1Γ (eV)	−0.22	−0.48	−0.55	−0.66
2Γ (eV)	−0.18	−0.36	−0.46	−0.58
1Δ (eV)	−0.12	−0.15	−0.19	−0.38
VBM (eV)	−0.81	−0.80	−0.80	−0.81
AS_{200}		−0.06	−0.05	−0.05

trates the placement of phosphorus atoms in 1/4 ML ordered [Fig. 1(b)] and disordered structures [Fig. 1(c)]. The most striking difference in the band structure is an avoided crossing between 1Γ and 1Δ that is present in the ordered structure but absent in the disordered case. Disorder also results in a reduced separation between the 1Γ, 2Γ, and 1Δ bands. We note that the QCT model[20] uses an averaged pseudopotential in the δ layer and thus implicitly describes the disordered case; the agreement between the QCT band structures and our Fig. 1(c) is excellent. This serves a twofold purpose: it validates the QCT approach and shows that a full DFT model can describe both ordered and disordered δ layers.

In summary, we have calculated the electronic structure of phosphorus δ-doped layers in silicon using a density-functional theory model in which both conduction-band and valence-band electrons are treated explicitly. We have demonstrated that calculated doping potentials, band energies, and donor-electron distributions are in good agreement with earlier predictions based on conduction-band-only models. Long-range interactions associated with a slowly decaying doping potential are adequately captured using a simple alignment shift with all of the qualitative characteristics of the band structure preserved.

This work was supported by the Australian Research Council, the Australian Government, and the U.S. Advanced Research and Development Activity, National Security Agency, and Army Research Office under Contract No. DAAD19-01-1-0653.

[1] H.-J. Gossmann and E. F. Schubert, Crit. Rev. Solid State Mater. Sci. **18**, 1 (1993).
[2] E. F. Schubert, *Delta-doping of Semiconductors* (Cambridge University Press, Cambridge, 1996).
[3] M. C. Qian, C. Y. Fong, K. Liu, W. E. Pickett, J. E. Pask, and L. H. Yang, Phys. Rev. Lett. **96**, 027211 (2006).
[4] H. Wu, P. Kratzer, and M. Scheffler, Phys. Rev. Lett. **98**, 117202 (2007).
[5] J. R. Tucker and T.-C. Shen, Int. J. Circuit Theory Appl. **28**, 553 (2000).
[6] B. E. Kane, Nature (London) **393**, 133 (1998).
[7] R. G. Clark, R. Brenner, T. M. Buehler, V. Chan, N. J. Curson, A. S. Dzurak, E. Gauja, H. S. Goan, A. D. Greentree, T. Hallam, A. R. Hamilton, L. C. L. Hollenberg, D. N. Jamieson, J. C. McCallum, G. J. Milburn, J. L. O'Brien, L. Oberbeck, C. I. Pake, S. D. Prawer, D. J. Reilly, F. J. Ruess, S. R. Schofield, M. Y. Simmons, F. E. Stanley, R. P. Starrett, C. Wellard, and C. Yang, Philos. Trans. R. Soc. London, Ser. A **361**, 1451 (2003).
[8] T.-C. Shen, J.-Y. Ji, M. A. Zudov, R.-R. Du, J. S. Kline, and J. R. Tucker, Appl. Phys. Lett. **80**, 1580 (2002).
[9] F. J. Ruess, L. Oberbeck, M. Y. Simmons, K. E. J. Goh, A. R. Hamilton, T. Hallam, S. R. Schofield, N. J. Curson, and R. G. Clark, Nano Lett. **4**, 1969 (2004).
[10] T.-C. Shen, J. S. Kline, T. Schenkel, S. J. Robinson, J.-Y. Ji, C. L. Yang, R. R. Du, and J. R. Tucker, J. Vac. Sci. Technol. B **22**, 3182 (2004).
[11] S. J. Robinson, J. S. Kline, H. J. Wheelwright, J. R. Tucker, C. L. Yang, R. R. Du, B. E. Volland, I. W. Rangelow, and T.-C. Shen, Phys. Rev. B **74**, 153311 (2006).
[12] W. Pok, T. C. G. Reusch, G. Scappucci, F. J. Ruess, A. R. Hamilton, and M. Y. Simmons, IEEE Trans. Nanotechnol. **6**, 213 (2007).
[13] F. J. Rueß, W. Pok, K. E. J. Goh, A. R. Hamilton, M. Y. Simmons, Phys. Rev. B **75**, 121303(R) (2007).
[14] F. J. Ruess, W. Pok, T. C. G. Reusch, M. J. Butcher, K. E. J. Goh, L. Oberbeck, G. Scappucci, A. R. Hamilton, and M. Y. Simmons, Small **3**, 563 (2007).
[15] M. Y. Simmons, F. J. Ruess, K. E. J. Goh, W. Pok, T. Hallam, M. J. Butcher, T. C. G. Reusch, G. Scappucci, A. R. Hamilton, and L. Oberbeck, Int. J. Nanotechnol. **5**, 352 (2008).
[16] I. Eisele, Superlattices Microstruct. **6**, 123 (1989).
[17] H.-M. Li, W.-X. Ni, M. Willander, K.-F. Berggren, B. E. Sernelius, and G. V. Hansson, Thin Solid Films **183**, 331 (1989).
[18] L. M. R. Scolfaro, D. Beliaev, R. Enderlein, and J. R. Leite, Phys. Rev. B **50**, 8699 (1994).
[19] A. L. Rosa, L. M. R. Scolfaro, R. Enderlein, G. M. Sipahi, and J. R. Leite, Phys. Rev. B **58**, 15675 (1998).
[20] G. Qian, Y.-C. Chang, and J. R. Tucker, Phys. Rev. B **71**, 045309 (2005).
[21] X. Cartoixà and Y.-C. Chang, Phys. Rev. B **72**, 125330 (2005).
[22] Test calculations with a highly truncated (12L) cell show differences of less than 0.005 Å. By using unrelaxed coordinates we eliminate oscillations in the doping potential.
[23] J. M. Soler, E. Artacho, J. D. Gale, A. Garcia, J. Junquera, P. Ordejon, and D. Sanchez-Portal, J. Phys.: Condens. Matter **14**, 2745 (2002).
[24] N. Troullier and J. L. Martins, Phys. Rev. B **43**, 1993 (1991).
[25] J. P. Perdew, K. Burke, and M. Ernzerhof, Phys. Rev. Lett. **77**, 3865 (1996).
[26] R. W. G. Wyckoff, *Crystal Structures* (Interscience, New York, 1963).